

1

2

3

Samuel R. Totorica^{1,2,3,4}, Amitava Bhattacharjee^{1,2,3,5}

¹Princeton Center for Heliophysics, Princeton, New Jersey 08543, USA

²Department of Astrophysical Sciences, Princeton University, Princeton, New Jersey 08544, USA

³Princeton Plasma Physics Laboratory, Princeton University, Princeton, New Jersey 08540, USA

⁴International Research Collaboration Center, National Institute of Natural Sciences, Tokyo 105-0001,
Japan

⁵Center for Computational Astrophysics, The Flatiron Institute, New York, New York 10010, USA

Key Points:

- For the first time, an exact kinetic magnetotail equilibrium is used to model magnetospheric substorm onset
- Comparing 2D and 3D simulations reveals the importance of the coupling between magnetic reconnection and the kinetic ballooning instability
- Self-consistent particle trajectories are analyzed for the first time in a realistic fully kinetic magnetotail configuration

Abstract

Magnetospheric substorms are preceded by a slow growth phase of magnetic flux loading and current sheet thinning in the tail. Extensive datasets have provided evidence of the triggering of instabilities at substorm onset, including magnetic reconnection and ballooning instabilities. Using an exact kinetic magnetotail equilibrium we present particle-in-cell simulations which capture the explosive nature of substorms through a disruption of the dipolarization front by the ballooning instability. We use self-consistent particle tracking to determine the nonthermal particle acceleration mechanisms.

Plain Language Summary

Magnetospheric substorms are events featuring bursty flows of magnetized plasma, highly energetic particles, and intense polar auroras. Substorms play a key role in the response of the magnetosphere to variations in the incoming solar wind. The Earth’s magnetic field lines are like elastic strings, and when they snap charged particles can be accelerated to high energies. Additionally, when there is enough plasma pressure pushing against the magnetic field, the magnetic field lines can develop an unstable oscillation known as a “ballooning instability” which is driven by the alignment of the plasma pressure gradient with magnetic field curvature. Using computer simulations that follow the trajectories of billions of particles in the Earth’s magnetosphere and compute their self-consistent electromagnetic forces, we show the importance of the interplay between reconnection and ballooning in the onset of substorms and acceleration of charged particles to high energies. These results have strong implications for the development of accurate models to predict space weather events and mitigate their damaging effects on critical infrastructure.

1 Introduction

The Earth’s magnetosphere is a complex environment involving the dynamics of magnetized, collisionless plasmas. The interaction with the incoming magnetized solar wind creates the interface regions of the bow shock and the downstream magnetosheath, and stretches the Earth’s magnetic field into an extended magnetotail on the night side of Earth. During times of suitable interplanetary magnetic field orientation, the solar wind plasma can enter the magnetosphere through magnetic reconnection, with excess energy and magnetic flux becoming stored in the magnetotail. This eventually leads to explosive disruptions known as substorms, where the magnetotail becomes unstable and violently releases the stored energy (Sitnov et al., 2019). Magnetospheric substorms can be frequent, occurring several times per day and associated with transient features such as bursty flows of magnetized plasma, nonthermal particle acceleration, and intensification of the polar aurora (Birn et al., 2012). Substorms play a key role in the global evolution of the magnetosphere and its response to the variable solar wind, and understanding their dynamics is critical for the development of accurate models for geomagnetic activity that can predict space weather events and mitigate their destructive impacts.

Critical unsolved problem in magnetotail physics include understanding the physical mechanisms that lead to the onset of substorms at near-Earth distances ($\sim 10R_E$, where R_E denotes the radius of the Earth) and the associated particle energization that leads to auroral intensification. Considering the magnetic field reversal across the magnetotail current sheet at mid-tail distances ($> 30R_E$) and the nature of observations such as intermittent bursts of plasma flows with enhanced electromagnetic fields, magnetic reconnection is widely believed to play an important role in the disruption of the magnetotail. Past work investigating the possibility of the onset of the tearing instability in the undisturbed magnetotail has faced difficulty due to the stabilizing effect of even weak normal (perpendicular to the reconnecting field in the reconnection plane, or N component in LMN current sheet coordinates) magnetic field components, which are present

in the curved field lines of the magnetotail (Schindler, 1974; Galeev & Zelenyĭ, 1976; Pritchett et al., 1991; Wang & Bhattacharjee, 1993; Pritchett, 1994). However, numerical simulations have shown that solar wind driving can lead to current sheet thinning and a reduction of the normal field, eventually surpassing a threshold that enables reconnection onset through collisionless tearing (Pritchett, 2005, 2010; Bessho & Bhattacharjee, 2014; Liu et al., 2014).

Free energy associated with the Earthward plasma pressure gradient indicates the additional possibility of three-dimensional cross-tail instabilities. Of particular interest, the aligned plasma pressure gradient and magnetic field curvature vectors can lead to the growth of the ballooning instability, which modulates the magnetic field orthogonal to the reconnection plane with linear growth rates that peak around wavelengths of $k_{\perp}\rho_i \sim \mathcal{O}(1)$ (Roux et al., 1991; Cheng & Lui, 1998). The ballooning instability could become destabilized as the magnetic field curvature increases from current sheet thinning, and may operate simultaneously with reconnection. It is believed that the inclusion of kinetic effects in models of ballooning is critical for explaining observations in the magnetotail, and that the region of highest instability is in the near-Earth dipole field transition region (Cheng & Lui, 1998; Cheng & Zaharia, 2004).

The details of how reconnection and/or ballooning lead to substorm onset and non-thermal particle acceleration in the collisionless plasmas of the type present in the magnetotail, and the interplay between near-earth and distant tail effects, are not yet fully understood. Observations give strong support for substorm onset auroral signatures being associated with an azimuthally localized disruption in the near-Earth dipole-tail transition region (Donovan et al., 2008; Sergeev et al., 2012), and the properties of the near-Earth disruption appear consistent with kinetic ballooning (Panov, Sergeev, et al., 2012; Panov, Nakamura, et al., 2012; Nishimura et al., 2016). Evidence exists for events with effects further in the tail (such as reconnection flows) preceding (Donovan et al., 2008) or following (Nishimura et al., 2016) the near-Earth disruption, indicating the possibility of multiple classes of substorms and onset mechanisms. Recently, 3D simulations are starting to be used to directly investigate the interaction of reconnection and ballooning (Vapirev et al., 2013; Sitnov et al., 2014; Zhu & Raeder, 2014; Lapenta et al., 2015; Zhu et al., 2017; Pritchett & Runov, 2017; Pritchett & Lu, 2018; Lu et al., 2018).

Initial conditions for simulations of the magnetotail have been a pervasive challenge due to the complex magnetic field geometry. Generalized Harris sheets that contain a small normal component of the magnetic field (Bessho & Bhattacharjee, 2014; Liu et al., 2014) are a suitable model for the distant tail but neglect the critical near-Earth region. Magnetohydrodynamic simulations can numerically relax to realistic field profiles (Hesse & Birn, 1993), however these are not Vlasov equilibria that could be used for kinetic simulations. While fluid models give important insight into global aspects of the magnetotail (Bhattacharjee et al., 1998b, 1998a; Birn et al., 1997; Zhu & Raeder, 2014), features of substorms firmly established by observations such as the kinetic scales of thin current sheets and the range of plasma beta and wavelengths over which instabilities are observed show the importance of kinetic dynamics in substorms. Fully kinetic simulations with realistic magnetic field profiles have previously been performed using a two-step procedure of first evolving ions in the fields as test particles, and then adding electrons at the locations of the ions (Pritchett & Lu, 2018). However, simulations that begin with initial conditions that are not rigorously in equilibrium have the potential to introduce transient flows that could influence the later development of the system. With a lack of rigorous initial conditions, highly idealized generalized Harris sheets remain the standard for kinetic magnetotail studies.

In this Letter, we investigate the onset of magnetospheric substorms using *ab initio* particle-in-cell (PIC) simulations (Birdsall & Langdon, 1985). Using the fully relativistic, state-of-the-art PIC code OSIRIS (Fonseca et al., 2002, 2008, 2013; Hemker, 2015), we perform fully kinetic and electromagnetic two- (2D) and three-dimensional (3D) sim-

ulations, for the first time starting from an *exact* kinetic equilibrium that captures both the near-Earth dipole magnetic field and the tail current sheet. Solar wind driving leads to current-sheet thinning and the onset of reconnection, producing dipolarization fronts and plasmoids that are ejected from the reconnection layer. Comparing 2D and 3D simulations allows the study of the complementary roles of reconnection and intrinsically 3D cross-tail instabilities, and their impacts on dipolarization fronts and substorm onset. We demonstrate that only in 3D, dipolarization fronts become disrupted as they travel into the near-Earth region as a result of the ballooning instability. Electrons and ions are accelerated to suprathermal energies and field-aligned currents traveling to the ionosphere are produced. These results reveal the importance of the coupling between reconnection and ballooning in the magnetotail and provide new insight into substorm onset.

2 Simulations

As emphasized above, a novel feature of our simulations is that we use as initial conditions an exact kinetic equilibrium that captures both the near-Earth dipole field and the extended tail current sheet. The equilibrium we employ was developed as an exact solution of the Grad-Shafranov equation using boundary conditions that approximate observations of the magnetotail field structure (Manankova, 2003; Yoon & Lui, 2005). Free parameters of the model include a factor γ that characterizes the relative strength of the dipole and tail magnetic fields, and the tail current sheet thickness δ . We choose a value of $\gamma = -3$ which gives the closest approximation to the commonly used model of Tsyganenko (Tsyganenko, 1989) while also not including an X point in the initial configuration. The initial current sheet thickness is chosen to be $\delta/d_i = 10$ (where d_i is the ion inertial length) which is in the range of typical values for the magnetotail and ensures initial stability of the tail. The number of ion inertial lengths per Earth radii is set to be $R_E/d_i = 5$. Along the x -axis, which points in the anti-sunward direction, the simulation domain extends from $x = 7-52R_E$, and of particular importance captures the dipole to tail transition region around $x \sim 10 - 12R_E$. The z -axis is aligned with the Earth's magnetic axis and has a length $L_z = 15R_E$. The simulations are run for $550\Omega_{ci}^{-1}$. For the 3D simulations, the total length of the out-of-plane y -dimension ranges from $L_y = 2.5-10.0R_E$, comparable to the typical cross-tail width of bursty bulk flows inferred from observations. The initial temperature ratio is set to be $T_i/T_e = 5$, following observations, and a background plasma is included with density $n_{bg} = 0.1$. The resolution of the spatial grid is $\Delta x/d_e = 0.5$, where d_e is the electron inertial length, and the number of particles per cell per species (electrons and ions) is $n_{ppc} = 16$ (128) in 3D (2D). To make the 3D simulations computationally feasible we use an artificial mass ratio of $m_e/m_i = 1/25$ and an Alfvén speed of $V_A/c = 0.1$, where V_A is calculated using the parameters of the tail current sheet.

To model the influence of solar wind driving, we apply an external electric field at the z boundaries that the z boundaries that drives plasma flows into the current layer (Liu et al., 2014; Bhattacharjee et al., 1998b, 1998a). The field profile along the z boundaries decays monotonically from the Earthward to tailward boundaries along x , and decays from the z boundaries to zero at $z = 0$ along x boundaries. The functional form defined only along the boundaries is given by $E_y(z, x) = |\sin(\pi z/L_z)| (0.5 + 0.5 \tanh(17 - 2.5x/R_E))$ where $E_0/V_A B_0 = 0.1$ and V_A and B_0 are the values corresponding to the lobe field. This field profile leads to reconnection onset at $x/R_E \approx 20$, in accordance with typical observations. The y dimension is periodic and the x and z boundaries are conducting for the electromagnetic fields and reflecting for the particles. In the absence of driving the simulations are confirmed to be stable.

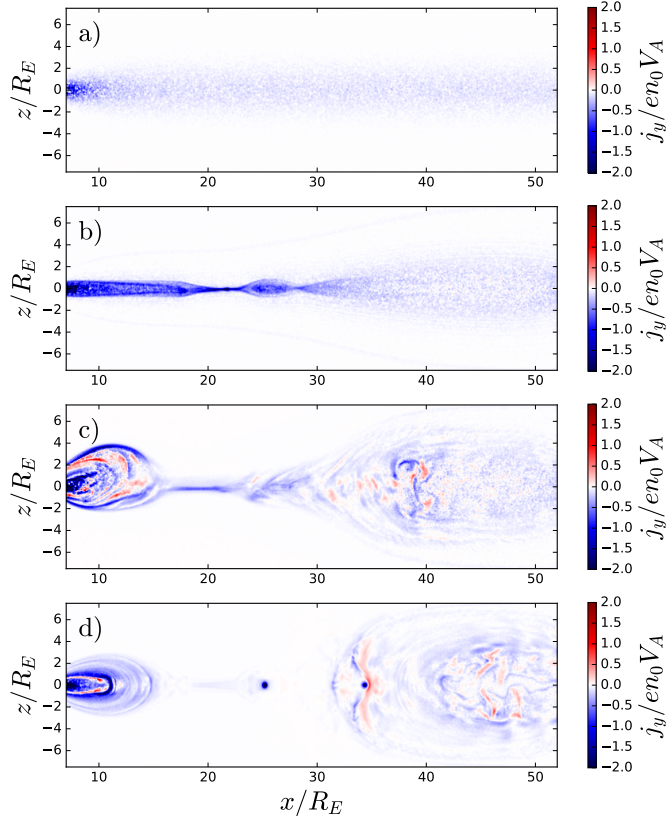


Figure 1. Cross-tail current density J_y in a 2D slice in $z-x$ of the 3D domain at (a) $\Omega_{ci}t = 0$, showing the initial equilibrium, (b) $\Omega_{ci}t = 449$ after reconnection onset, showing plasmoids and the dipolarization front propagating Earthwards, and (c) $\Omega_{ci}t = 520$ showing the disruption of the dipolarization front and flapping of the reconnecting current sheet. (d) shows a 2D simulation at $\Omega_{ci}t = 520$ for comparison.

3 Results

The evolution of the 3D simulation is illustrated in Figure 1, which shows a 2D slice of the cross-tail current density in the $x-z$ plane at three different times. The external electric field at the z boundaries drives magnetic flux and plasma flows towards the center of the current sheet at $z = 0$, leading to thinning of the current sheet and the eventual onset of reconnection once it reaches a scale on the order of d_e . The thin current sheet where reconnection occurs shows growing oscillations in the z -direction, which correspond to the current sheet flapping motions that have been observed by satellites and in simulations (Sergeev et al., 2003; Runov et al., 2005; Petrukovich et al., 2006; Sharma et al., 2008; Runov et al., 2009; Sitnov et al., 2014; Wei et al., 2019). The characteristic length scale of the wavelength and amplitude is seen to be on the order of R_E , similar to observations (Sergeev et al., 2003; Petrukovich et al., 2006; Runov et al., 2009). Reconnection results in both Earthward and tailward plasma flows, and the formation of several plasmoids / flux ropes that are ejected both Earthward and tailward. After the initial onset of reconnection there is an intense layer of current that travels Earthward that is associated with a sharp rise in the normal component of the magnetic field B_z over a length scale $\sim d_i$. This corresponds to the dipolarization fronts which are often seen in observations (Angelopoulos et al., 1992). The layer becomes disturbed as it enters the near-Earth dipole field region around $x/R_E = 10-12$ and is eventually disrupted by a cross-tail instability. In analogous 2D simulations in the $x-z$ plane where reconnection occurs without cross-tail instabilities, the dipolarization front remains at the end of the simulation.

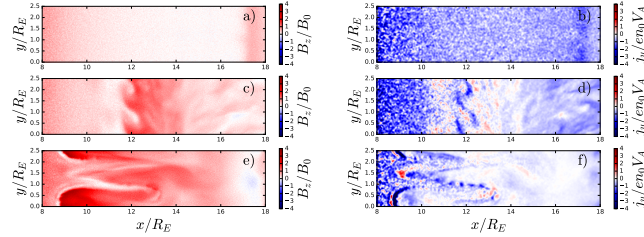


Figure 2. 2D slices in the equatorial $y - x$ plane at $z = 0$ of the normal component of the magnetic field B_z (a,c,e) and the cross-tail current density J_y (b,d,f) at three times. (a,b) At $\Omega_{ci}t = 449$, the dipolarization front propagates stably towards the Earth. (c,d) At $\Omega_{ci}t = 484$, the dipolarization front enters the near-Earth region and begins to show modulations. (e,f) At $\Omega_{ci}t = 520$ the nonlinear growth of the instability has resulted in a disruption of the dipolarization front.

To understand the 3D mechanism of the dipolarization front disruption, Figure 2 shows the dynamics in the equatorial $x - y$ plane at $z = 0$, showing the evolution of the normal component of the magnetic field B_z and the cross tail current density J_y . The early time clearly shows the current layer of the dipolarization front supporting the sharp increase in magnetic flux from the reconnection outflows over a length scale of $\sim d_i$, consistent with observations. The dipolarization front maintains its stability as it travels from the reconnection layer through the distant tail-region. Once it reaches the transition region where the Earth’s dipole field becomes significant, the dipolarization front begins to show growing modulations. At later times the current layer associated with the dipolarization front is seen to disrupt and become disconnected in the near-Earth region. The characteristic length scales of the growing modes are $k_y \rho_i \approx 1$, which together with the disruption in the near-Earth region and the associated field-aligned cur-

rents (described below) indicates that this is the result of the kinetic ballooning instability (Cheng & Lui, 1998; Cheng & Zaharia, 2004). Comparing to simulations with $L_y/R_E = 5$ and 10 , the length scale of the dominant mode and onset location of $x \approx 15R_E$ are found to be insensitive to the limited system size in the y -direction (Figure S1 in Supporting Information). The $L_y/R_E = 10$ simulation additionally develops a localized tailward breakout with a width of $\Delta_y/R_E \sim 4$, which may be related to reconnection onset occurring slightly further along the tail in this simulation and will be investigated in further detail in future work. As the dipolarization front and associated plasma and magnetic field travel Earthward, the Earthward pressure gradient builds up to $L_P = |P/\nabla P| \sim 0.5R_e$. For substorm conditions derived from observations including $L_P \sim 0.5R_e$ and $k_y\rho_i = 1$, the growth rate of the kinetic ballooning instability was calculated to be approximately $\omega_{KBI} = 0.1s^{-1}$ or $\omega_{ci}/\omega_{KBI} \approx 50$ using ω_{ci} for a magnetic field of $B = 10$ nT (Cheng & Lui, 1998). The disruption of the dipolarization front takes place over a timescale $\omega_{ci}t \sim 50$ (Figure 2) and is thus consistent with a growth rate of the order of magnitude of that expected for the kinetic ballooning instability. Figure 3 shows how the disruption is occurring in a region where the plasma beta exceeds the critical value of $\beta_c = 50$, consistent with the kinetic ballooning instability (Cheng & Lui, 1998). This mechanism is distinct from the BICI mode (Pritchett & Coroniti, 2010, 2011, 2013) which has $k_y\rho_i \gg 1$ and requires a small plasma beta. The strong magnetization of the electrons in the dipolarization front precludes spurious numerical effects from the artificial mass ratio such as an artificial ion-electron drift-kink mode (Daughton, 1999). A physical ion-ion kink mode from the initially stationary background plasma used in the simulation could potentially contribute to the disruption depending on the specific value chosen for the background plasma density.

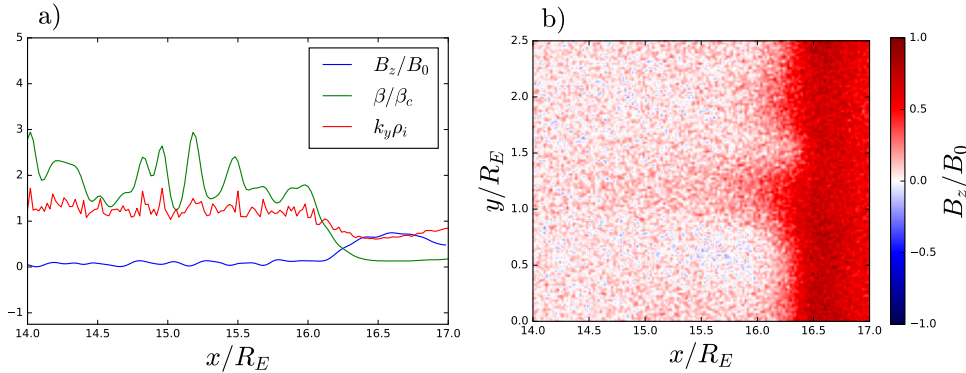


Figure 3. a) Normal component of the magnetic field B_z normalized to the characteristic field strength of the tail current sheet B_0 , plasma beta normalized to the critical value of $\beta_c = 50$ for the onset of the kinetic ballooning instability, and $k_y\rho_i$ of the instability in the near Earth region of the simulation. b) B_z component of the magnetic field in the near-Earth region of the equatorial plane. Analysis is performed at $\Omega_{ci}t = 456$.

One of the most dramatic and readily observed signatures of substorms is the intensification of the aurora that results from charged particles impinging on the ionosphere (Birn et al., 2012). The parallel component of the current J_{\parallel} shows Earthward traveling field-aligned currents originating at the dipolarization front that intensify as the dipolarization front is disrupted. These field-aligned currents travel to the Earthward boundary, and in an open system could continue to travel and impact the ionosphere and give rise to the auroral intensification characteristic of substorms. Nonthermal energetic electrons and ions are also commonly observed in association with substorm onset. Parti-

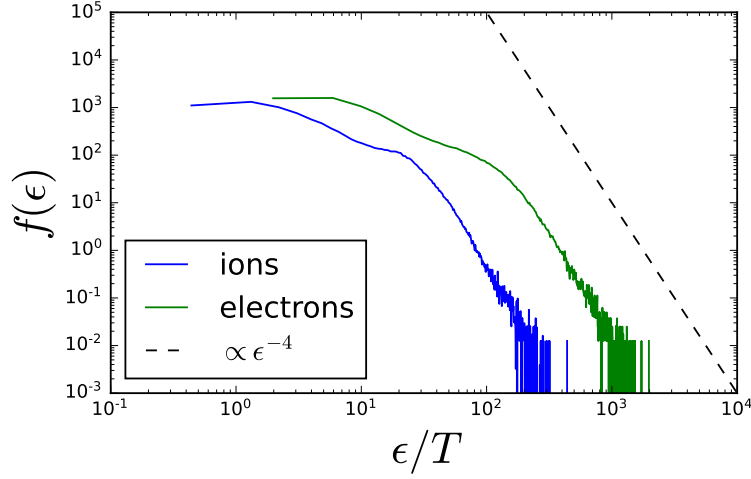


Figure 4. Electron and ion energy spectra at $\Omega_{ci}t = 534$ integrated across y within a square region of 1 ion skin depth width centered at $x = 11 R_E, z = 0.0 R_E$. A power-law energy spectrum with index $p = -4$ plotted as reference.

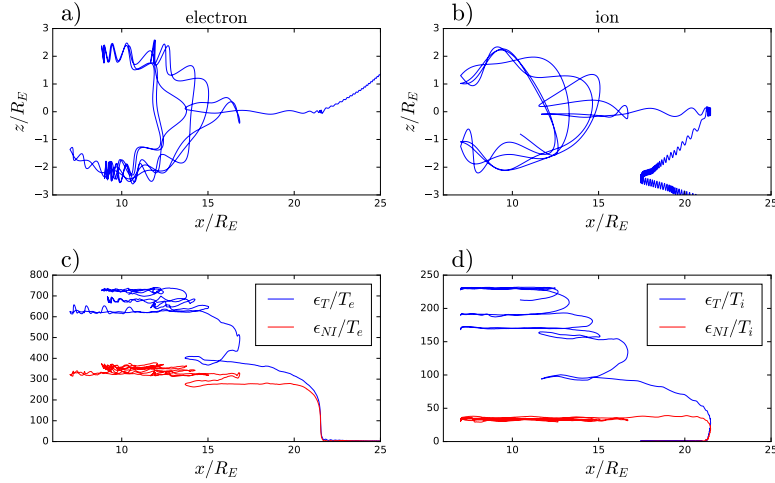


Figure 5. Particle trajectories for a representative energetic electron (a,c) and ion (b,d). (a) and (b) show the trajectories in the x - z plane and (c) and (d) show the total particle energies ϵ_T and the energy gained from the nonideal electric field ϵ_{NI} as a function of position along x . The electron and ion first enter the plotted subdomain at $\Omega_{ci}t = 465$ and $\Omega_{ci}t = 165$, respectively, and the trajectories are plotted until $\Omega_{ci}t = 549$.

cles are known to be energized both in the vicinity of the reconnection site (Moebius et al., 1983; Øieroset et al., 2002; Imada et al., 2005, 2011, 2015a) and in the near-Earth region (Baker et al., 1981; Birn et al., 1997; Birn, 1997) (referred to as substorm injections). To investigate the particle acceleration resulting from the disruption of the dipolarization front, Figure 4 shows the electron and ion energy spectra integrated over a square region of 1 ion skin depth width centered at $x = 11 R_E, z = 0.0 R_E$. As the dipolarization front crosses into the near-Earth region and becomes disrupted, both electrons and ions show strong energization. The spectra are normalized to the initial thermal energy of each species, and the most energetic particles are seen to reach more than 100 times the initial thermal energy. In physical units these electrons are reaching energies of approximately $\sim 100\text{keV}$, and the highest energy portion of the spectrum resembles a power law with an index of ~ 4 over a limited energy range. This compares favorably with recent satellite measurements of energetic electron and ion acceleration in the magnetotail (Imada et al., 2015b; Turner et al., 2016).

To determine the physical mechanisms leading to the acceleration of the energetic particles we have performed self-consistent tracking of the trajectories of a sample of the most energetic ions and electrons from the 2D simulation. Figure 5 shows the evolution of a typical energetic electron, with its trajectory in the $x-z$ plane in Figure 5 (a) and its total energy ϵ_T as function of x in Figure 5 (c) (blue). The electron first gains a significant amount of energy from the reconnection electric field as it enters the current sheet near the X point. It is then directed earthward by the magnetic field and begins to travel along the Earth’s dipolar field lines and experience mirror reflections as it approaches the polar regions. The electron continues to gain energy from betatron acceleration as magnetic flux piles up from the Earthward travelling reconnection flows. Electrons that reach the dipolar field lines with larger pitch angles are confined closer to the equatorial plane where the cross tail electric field resulting from the flux pileup is greatest, and are accelerated at a greater rate. Other trajectories also show electrons can become trapped inside plasmoids and gain energy in a Fermi acceleration process as they bounce between the ends of the plasmoid (Drake et al., 2006) which are ejected and absorbed into the Earth’s dipole field by a secondary reconnection processes. The acceleration mechanisms for energetic ions are similar, and a representative example is shown in Figures 5 (b) and (d). Ions are also seen to gain energy from the reconnection electric field at the X point and inside plasmoids. Additionally, the large gyroradii of the ions allows them to be reflected upstream into the reconnection flows (Figure 5 (d)) and further gain energy from the enhanced cross tail electric field in the magnetized plasma flow. The red lines in Figure 5 (b) and (d) show the energy gained from the nonideal component of the electric field \mathbf{E}_{NI} , calculated self-consistently within the simulation as $\mathbf{E}_{NI} = \mathbf{E} + \mathbf{V} \times \mathbf{B}$, where \mathbf{V} is the plasma fluid velocity. The initial energy gain from the X points comes largely from the nonideal field, while the remaining energy gain during mirror reflections comes almost entirely from the ideal field. This shows the importance of kinetic effects for modelling particle acceleration in the magnetotail, but lends support to methods that couple global fluid models to kinetic models in certain regions of the domain. These results confirm major conclusions of previous theoretical and test particle studies of particle acceleration in the magnetotail (Birn et al., 2012), for the first time in a self-consistent fully kinetic simulation.

4 Conclusion

In conclusion, we have implemented a novel configuration of an exact kinetic equilibrium that captures the dipole to tail transition and reproduces the salient features observed in the magnetotail. Solar wind driving leads to thin current sheet formation and the onset of reconnection, resulting in intermittent plasma flows, plasmoid formation and ejection, and current sheet flapping. Earthward traveling dipolarization fronts are formed in both 2D and 3D simulations, but only in 3D the dipolarization front is disrupted in

the near-Earth region by the ballooning instability. Field-aligned currents and nonthermal ions and electrons are accelerated, and particle tracking has determined the dominant acceleration mechanisms. Future work will involve incorporating these dynamics into global magnetosphere simulations for predictive space weather modelling.

Data availability statement

Simulation data is hosted on the Zenodo repository and can be accessed at <https://zenodo.org/record/8310560> (DOI 10.5281/zenodo.8310560) (Totorica & Bhattacharjee, 2023).

Acknowledgments

The authors acknowledge the OSIRIS Consortium, consisting of UCLA and IST (Portugal) for the use of the OSIRIS 4.0 framework. S.T. was supported by the NASA Jack Eddy Postdoctoral Fellowship and the Max-Planck Princeton Center. Simulations were performed on Perlmutter (NERSC), Mira and Theta (ALCF) and Bluewaters (NCSA).

References

- Angelopoulos, V., Baumjohann, W., Kennel, C. F., Coroniti, F. V., Kivelson, M. G., Pellat, R., ... Paschmann, G. (1992). Bursty bulk flows in the inner central plasma sheet. *Journal of Geophysical Research*, *97*(A4), 4027. doi: 10.1029/91ja02701
- Baker, D. N., Hones, E. W., Higbie, P. R., & Belian, R. D. (1981). Global Properties of the Magnetosphere During a Substorm Growth Phase ' A Case Study term is one a very This of dynamical Large-scale agreement exists from theoretical topology about the is transferred precipitation one required to power all of Reduced to. *October*, *86*(1), 8941–8956.
- Bessho, N., & Bhattacharjee, A. (2014). Instability of the current sheet in the Earth's magnetotail with normal magnetic field. *Physics of Plasmas*, *21*(10), 1–7. doi: 10.1063/1.4899043
- Bhattacharjee, A., Ma, Z. W., & Wang, X. (1998a). Ballooning instability of a thin current sheet in the high-Lundquist-number magnetotail. *Geophysical Research Letters*, *25*(6), 861–864. doi: 10.1029/98GL00412
- Bhattacharjee, A., Ma, Z. W., & Wang, X. (1998b). Dynamics of thin current sheets and their disruption by ballooning instabilities: A mechanism for magnetospheric substorms. *Physics of Plasmas*, *5*(5), 2001–2009. doi: 10.1063/1.872871
- Birdsall, C., & Langdon, A. (1985). *Plasma Physics via Computer Simulation*. McGraw-Hill.
- Birn, J. (1997). Characteristic plasma properties during dispersionless substorm injections at geosynchronous orbit. *Journal of Geophysical Research A: Space Physics*, *102*(A2), 2309–2324. doi: 10.1029/96JA02870
- Birn, J., Artemyev, A. V., Baker, D. N., Echim, M., Hoshino, M., & Zelenyi, L. M. (2012). Particle acceleration in the magnetotail and aurora. *Space Science Reviews*, *173*(1-4), 49–102. doi: 10.1007/s11214-012-9874-4
- Birn, J., Thomsen, M. F., Borovsky, J. E., Reeves, G. D., McComas, D. J., Belian, R. D., & Hesse, M. (1997). Substorm ion injections: Geosynchronous observations and test particle orbits in three-dimensional dynamic MHD fields. *Journal of Geophysical Research A: Space Physics*, *102*(A2), 2325–2341. doi: 10.1029/96JA03032
- Cheng, C. Z., & Lui, A. T. (1998). Kinetic ballooning instability for substorm onset and current disruption observed by AMPTE/CCE. *Geophysical Research Letters*, *25*(21), 4091–4094. doi: 10.1029/1998GL900093

- Cheng, C. Z., & Zaharia, S. (2004). MHD ballooning instability in the plasma sheet. *Geophysical Research Letters*, *31*(6), 10–13. doi: 10.1029/2003gl018823
- Daughton, W. (1999). The unstable eigenmodes of a neutral sheet. *Physics of Plasmas*, *6*(4), 1329. Retrieved from <http://scitation.aip.org/content/aip/journal/pop/6/4/10.1063/1.873374> doi: 10.1063/1.873374
- Donovan, E., Liu, W., Liang, J., Spanswick, E., Voronkov, I., Connors, M., ... Rae, I. J. (2008). Simultaneous THEMIS in situ and auroral observations of a small substorm. *Geophysical Research Letters*, *35*(17), 1–5. doi: 10.1029/2008GL033794
- Drake, J. F., Swisdak, M., Che, H., & Shay, M. A. (2006, oct). Electron acceleration from contracting magnetic islands during reconnection. *Nature*, *443*(7111), 553–556. Retrieved from <http://www.ncbi.nlm.nih.gov/pubmed/17024088> doi: 10.1038/nature05116
- Fonseca, R. A., Martins, S. F., Silva, L. O., Tonge, J. W., Tsung, F. S., & Mori, W. B. (2008, dec). One-to-one direct modeling of experiments and astrophysical scenarios: pushing the envelope on kinetic plasma simulations. *Plasma Physics and Controlled Fusion*, *50*(12), 124034. Retrieved from <http://stacks.iop.org/0741-3335/50/i=12/a=124034?key=crossref.59dd49a28f003047851fb0c781d5fcd><http://arxiv.org/abs/0810.2460><http://stacks.iop.org/0741-3335/50/i=12/a=124034?key=crossref.59dd49a28f003047851fb0c781d5fcd>{\%}5Cn<http://arxiv.org/abs/0810.2460> doi: 10.1088/0741-3335/50/12/124034
- Fonseca, R. A., Silva, L. O., Tsung, F. S., Decyk, V. K., Lu, W., Ren, C., ... Adam, J. C. (2002). OSIRIS: A Three-Dimensional, Fully Relativistic Particle in Cell Code for Modeling Plasma Based Accelerators. *Lect. Notes Comput. Sci.*, *2331*, 342–351. Retrieved from http://link.springer.com/chapter/10.1007/3-540-47789-6{_}36http://link.springer.com/10.1007/3-540-47789-6{_}36{\%}5Cn<http://www.springerlink.com/content/0p7ulb2dm9441glq/{\%}5Cn><http://www.springerlink.com/content/0p7ulb2dm9441glq/fulltext.pdf{\%}5Cn><http://link.springer.com> doi: 10.1007/3-540-47789-6_36
- Fonseca, R. A., Vieira, J., Fiuza, F., Davidson, A., Tsung, F. S., Mori, W. B., & Silva, L. O. (2013, dec). Exploiting multi-scale parallelism for large scale numerical modelling of laser wakefield accelerators. *Plasma Physics and Controlled Fusion*, *55*(12), 124011. Retrieved from <http://stacks.iop.org/0741-3335/55/i=12/a=124011?key=crossref.96a8cddb9b5024abacb36e3d8610727> doi: 10.1088/0741-3335/55/12/124011
- Galeev, A., & Zelenyĭ, L. (1976). Tearing instability in plasma configurations. *Soviet Journal of Experimental and Theoretical Physics*, *43*(6), 1113.
- Hemker, R. G. (2015). Particle-In-Cell Modeling of Plasma-Based Accelerators in Two and Three Dimensions. *arXiv*. Retrieved from <http://arxiv.org/abs/1503.00276>
- Hesse, M., & Birn, J. (1993). Three-dimensional magnetotail equilibria by numerical relaxation techniques. *Journal of Geophysical Research*, *98*(A3), 3973. Retrieved from <http://doi.wiley.com/10.1029/92JA02905> doi: 10.1029/92JA02905
- Imada, S., Hirai, M., & Hoshino, M. (2015a). Energetic ion acceleration during magnetic reconnection in the Earth’s magnetotail Space science. *Earth, Planets and Space*, *67*(1), 203. Retrieved from <http://dx.doi.org/10.1186/s40623-015-0372-2> doi: 10.1186/s40623-015-0372-2
- Imada, S., Hirai, M., & Hoshino, M. (2015b). Energetic ion acceleration during magnetic reconnection in the earth’s magnetotail space science. *Earth, Planets and Space*, *67*. Retrieved from <http://dx.doi.org/10.1186/s40623-015-0372-2> doi: 10.1186/s40623-015-0372-2

- Imada, S., Hirai, M., Hoshino, M., & Mukai, T. (2011). Favorable conditions for energetic electron acceleration during magnetic reconnection in the Earth's magnetotail. *Journal of Geophysical Research: Space Physics*, *116*(8), 1–13. doi: 10.1029/2011JA016576
- Imada, S., Hoshino, M., & Mukai, T. (2005). Average profiles of energetic and thermal electrons in the magnetotail reconnection regions. *Geophysical Research Letters*, *32*(9), 1–4. doi: 10.1029/2005GL022594
- Lapenta, G., Markidis, S., Goldman, M. V., & Newman, D. L. (2015). Secondary reconnection sites in reconnection-generated flux ropes and reconnection fronts. *Nature Physics*, *11*(8), 690–695. doi: 10.1038/nphys3406
- Liu, Y. H., Birn, J., Daughton, W., Hesse, M., & Schindler, K. (2014). Onset of reconnection in the near magnetotail: PIC simulations. *Journal of Geophysical Research: Space Physics*, *119*(12), 9773–9789. doi: 10.1002/2014JA020492
- Lu, S., Pritchett, P. L., Angelopoulos, V., & Artemyev, A. V. (2018). Formation of Dawn-Dusk Asymmetry in Earth's Magnetotail Thin Current Sheet: A Three-Dimensional Particle-In-Cell Simulation. *Journal of Geophysical Research: Space Physics*, *123*(4), 2801–2814. doi: 10.1002/2017JA025095
- Manankova, A. V. (2003). Two-dimensional current-carrying plasma sheet in the near-Earth geomagnetic tail region: A quasi-stationary evolution. *Annales Geophysicae*, *21*(12), 2259–2269. doi: 10.1007/BF03391870
- Moebius, E., Scholer, M., Hovestadt, D., & Paschmann, G. (1983). Energetic Particles in the Vicinity of a Possible Neutral Line in the Plasma Sheet. *Journal of Geophysical Research*, *88*(A10), 7742–7752. doi: 10.1029/ja088ia10p07742
- Nishimura, Y., Yang, J., Pritchett, P. L., Coroniti, F. V., Donovan, E. F., Lyons, L. R., ... Mende, S. B. (2016). Statistical properties of substorm auroral onset beads/rays. *Journal of Geophysical Research: Space Physics*, *121*(9), 8661–8676. doi: 10.1002/2016JA022801
- Øieroset, M., Lin, R. P., Phan, T. D., Larson, D. E., & Bale, S. D. (2002). Evidence for Electron Acceleration up to [Formula presented] in the Magnetic Reconnection Diffusion Region of Earth's Magnetotail. *Physical Review Letters*, *89*(19), 1–4. doi: 10.1103/PhysRevLett.89.195001
- Panov, E. V., Nakamura, R., Baumjohann, W., Kubyshkina, M. G., Artemyev, A. V., Sergeev, V. A., ... Larson, D. (2012). Kinetic ballooning/interchange instability in a bent plasma sheet. *Journal of Geophysical Research: Space Physics*, *117*(6), 1–22. doi: 10.1029/2011JA017496
- Panov, E. V., Sergeev, V. A., Pritchett, P. L., Coroniti, F. V., Nakamura, R., Baumjohann, W., ... McFadden, J. P. (2012). Observations of kinetic ballooning/interchange instability signatures in the magnetotail. *Geophysical Research Letters*, *39*(8), 2–7. doi: 10.1029/2012GL051668
- Petrukovich, A. A., Zhang, T. L., Baumjohann, W., Nakamura, R., Runov, A., Balogh, A., & Carr, C. (2006). Oscillatory magnetic flux tube slippage in the plasma sheet. *Annales Geophysicae*, *24*(6), 1695–1704. doi: 10.5194/angeo-24-1695-2006
- Pritchett, P. L. (1994). Effect of electron dynamics on collisionless reconnection in two-dimensional magnetotail equilibria. *Journal of Geophysical Research*, *99*(A4), 5935. doi: 10.1029/93ja03297
- Pritchett, P. L. (2005). Externally driven magnetic reconnection in the presence of a normal magnetic field. *Journal of Geophysical Research: Space Physics*, *110*. doi: 10.1029/2004JA010948
- Pritchett, P. L. (2010). Onset of magnetic reconnection in the presence of a normal magnetic field: Realistic ion to electron mass ratio. *Journal of Geophysical Research: Space Physics*, *115*(10), 1–9. doi: 10.1029/2010JA015371
- Pritchett, P. L., & Coroniti, F. V. (2010). A kinetic ballooning/interchange instability in the magnetotail. *Journal of Geophysical Research: Space Physics*, *115*. doi: 10.1029/2009JA014752

- Pritchett, P. L., & Coroniti, F. V. (2011, 5). Plasma sheet disruption by interchange-generated flow intrusions. *Geophysical Research Letters*, *38*, n/a-n/a. doi: 10.1029/2011gl047527
- Pritchett, P. L., & Coroniti, F. V. (2013). Structure and consequences of the kinetic ballooning/interchange instability in the magnetotail. *Journal of Geophysical Research: Space Physics*, *118*, 146-159. doi: 10.1029/2012JA018143
- Pritchett, P. L., Coroniti, F. V., Pellat, R., & Karimabadi, H. (1991). Collisionless reconnection in two-dimensional magnetotail equilibria. *Journal of Geophysical Research*, *96*(91), 11523-11538. doi: 10.1029/91JA01094
- Pritchett, P. L., & Lu, S. (2018). Externally Driven Onset of Localized Magnetic Reconnection and Disruption in a Magnetotail Configuration. *Journal of Geophysical Research: Space Physics*, *123*(4), 2787-2800. doi: 10.1002/2017JA025094
- Pritchett, P. L., & Runov, A. (2017). The interaction of finite-width reconnection exhaust jets with a dipolar magnetic field configuration. *Journal of Geophysical Research: Space Physics*, *122*(3), 3183-3200. doi: 10.1002/2016JA023784
- Roux, A., Perraut, S., Robert, P., Morane, A., Pedersen, A., Korth, A., ... Pellinen, R. (1991). Plasma sheet instability related to the westward traveling surge. *Journal of Geophysical Research*, *96*(A10), 17697. doi: 10.1029/91ja01106
- Runov, A., Angelopoulos, V., Sergeev, V. A., Glassmeier, K. H., Auster, U., McFadden, J., ... Mann, I. (2009). Global properties of magnetotail current sheet flapping: THEMIS perspectives. *Annales Geophysicae*, *27*(1), 319-328. doi: 10.5194/angeo-27-319-2009
- Runov, A., Sergeev, V. A., Baumjohann, W., Nakamura, R., Apatenkov, S., Asano, Y., ... Rème, H. (2005). Electric current and magnetic field geometry in flapping magnetotail current sheets. *Annales Geophysicae*, *23*(4), 1391-1403. doi: 10.5194/angeo-23-1391-2005
- Schindler, K. (1974). A theory of the substorm mechanism. *Journal of Geophysical Research*, *79*(19), 2803-2810. doi: 10.1029/ja079i019p02803
- Sergeev, V., Nishimura, Y., Kubyshkina, M., Angelopoulos, V., Nakamura, R., & Singer, H. (2012). Magnetospheric location of the equatorward prebreakup arc. *Journal of Geophysical Research: Space Physics*, *117*(1), 1-18. doi: 10.1029/2011JA017154
- Sergeev, V., Runov, A., Baumjohann, W., Nakamura, R., Zhang, T. L., Volwerk, M., ... Klecker, B. (2003). Current sheet flapping motion and structure observed by Cluster. *Geophysical Research Letters*, *30*(6), 2-5. doi: 10.1029/2002GL016500
- Sharma, A. S., Nakamura, R., Runov, A., Grigorenko, E. E., Hasegawa, H., Hoshino, M., ... Snekvik, K. (2008). Transient and localized processes in the magnetotail: A review. *Annales Geophysicae*, *26*(4), 955-1006. doi: 10.5194/angeo-26-955-2008
- Sitnov, M. I., Birn, J., Ferdousi, B., Gordeev, E., Khotyaintsev, Y., Merkin, V., ... Zhou, X. (2019). Explosive Magnetotail Activity. *Space Science Reviews*, *215*(4). Retrieved from <http://dx.doi.org/10.1007/s11214-019-0599-5> doi: 10.1007/s11214-019-0599-5
- Sitnov, M. I., Merkin, V. G., Swisdak, M., Motoba, T., Buzulukova, N., Moore, T. E., ... Ohtani, S. (2014). Magnetic reconnection, buoyancy, and flapping motions in magnetotail explosions. *Journal of Geophysical Research: Space Physics*, *119*(9), 7151-7168. doi: 10.1002/2014JA020205
- Torica, S., & Bhattacharjee, A. (2023). Interplay of three-dimensional instabilities and magnetic reconnection in the explosive onset of magnetospheric substorms [dataset]. *Zenodo*. (<https://zenodo.org/record/8310560>) doi: 10.5281/zenodo.8310560
- Tsyganenko, N. A. (1989). A magnetospheric magnetic field model with a warped tail current sheet. *Planetary and Space Science*, *37*(1), 5-20. doi: 10.1016/

0032-0633(89)90066-4

- Turner, D. L., Fennell, J. F., Blake, J. B., Clemmons, J. H., Mauk, B. H., Cohen, I. J., . . . Burch, J. L. (2016). Energy limits of electron acceleration in the plasma sheet during substorms: A case study with the Magnetospheric Multi-scale (MMS) mission. *Geophysical Research Letters*, *43*(15), 7785–7794. doi: 10.1002/2016GL069691
- Vapirev, A. E., Lapenta, G., Divin, A., Markidis, S., Henri, P., Goldman, M., & Newman, D. (2013). Formation of a transient front structure near reconnection point in 3-D PIC simulations. *Journal of Geophysical Research: Space Physics*, *118*(4), 1435–1449. doi: 10.1002/jgra.50136
- Wang, X., & Bhattacharjee, A. (1993). Global asymptotic equilibria and collisionless tearing stability of magnetotail plasmas. *Journal of Geophysical Research: Space Physics*, *98*(A11), 19419–19434. doi: 10.1029/93ja01153
- Wei, Y. Y., Huang, S. Y., Rong, Z. J., Yuan, Z. G., Jiang, K., Deng, X. H., . . . Deng, D. (2019). Observations of Short-period Current Sheet Flapping Events in the Earth’s Magnetotail. *The Astrophysical Journal*, *874*(2), L18. doi: 10.3847/2041-8213/ab0f28
- Yoon, P. H., & Lui, A. T. (2005). A class of exact two-dimensional kinetic current sheet equilibria. *Journal of Geophysical Research: Space Physics*, *110*(A1), 1–9. doi: 10.1029/2003JA010308
- Zhu, P., Bhattacharjee, A., Sangari, A., Wang, Z., & Bonofiglio, P. (2017). Three-dimensional geometry of magnetic reconnection induced by ballooning instability in a generalized Harris sheet. *Physics of Plasmas*, *24*(2). Retrieved from <http://dx.doi.org/10.1063/1.4976994> doi: 10.1063/1.4976994
- Zhu, P., & Raeder, J. (2014). Ballooning instability-induced plasmoid formation in near-Earth plasma sheet. *Journal of Geophysical Research: Space Physics*, *119*(1), 131–141. doi: 10.1002/2013JA019511